



# Quantifying uncertainties on the solution model of seismic tomography

Carole Duffet, Delphine Sinoquet

## ► To cite this version:

Carole Duffet, Delphine Sinoquet. Quantifying uncertainties on the solution model of seismic tomography. European Congress on Computational Methods in Applied Sciences and Engineering, Jul 2004, Jyvaskyla, Finland. pp.24 - 28. hal-02284262

HAL Id: hal-02284262

<https://ifp.hal.science/hal-02284262>

Submitted on 11 Sep 2019

**HAL** is a multi-disciplinary open access archive for the deposit and dissemination of scientific research documents, whether they are published or not. The documents may come from teaching and research institutions in France or abroad, or from public or private research centers.

L'archive ouverte pluridisciplinaire **HAL**, est destinée au dépôt et à la diffusion de documents scientifiques de niveau recherche, publiés ou non, émanant des établissements d'enseignement et de recherche français ou étrangers, des laboratoires publics ou privés.

## QUANTIFYING UNCERTAINTIES ON THE SOLUTION MODEL OF SEISMIC TOMOGRAPHY

Carole DUFFET\* and Delphine SINOQUET†

\*Geophysics division  
e-mail: carole.duffet@ifp.fr

† Technology, computer Science, and Applied Mathematics Division  
1-4 avenue de Bois-Préau, 92500 Rueil-Malmaison, France  
e-mail: delphine.sinoquet@ifp.fr

**Key words:** Tomography, uncertainties quantification, velocity model building

**Abstract.** *Reflection tomography allows the determination of a velocity model that fits the traveltime data associated with reflections of seismic waves in the subsurface. A least-square formulation is used to compare the observed traveltimes and the traveltimes computed by the forward operator based on a ray tracing. This non linear optimization problem is solved classically by a Gauss-Newton method based on successive linearizations of the forward operator. The obtained solution is only one among many possible models. Indeed, the uncertainties on the observed traveltimes (resulting from an interpretative event picking on seismic records) and more generally the underdetermination of the inverse problem lead to uncertainties on the solution. An a posteriori uncertainty analysis is then crucial to delimit the range of possible solutions that fit, with the expected accuracy, the data and the a priori information. A linearized a posteriori analysis is possible by an analysis of the a posteriori covariance matrix, inverse of the Gauss-Newton approximation of the matrix. The computation of this matrix is generally expensive (the matrix is huge for 3D problems) and the physical interpretation of the results is difficult. Then we propose a formalism which allows to compute uncertainties on relevant geological quantities for a reduced computational time. Nevertheless, this approach is only valid in the vicinity of the solution model (linearized framework) and complex cases may require a non linear approach. An application on a 2D real data set illustrates the linearized approach to quantify uncertainties on the solution of seismic tomography and the limitations of this approach are discussed.*

## 1 INTRODUCTION

Geophysical methods for imaging complex geological subsurface in petroleum exploration requires the determination of an accurate propagation velocity model. Seismic reflection tomography ([1]) turns out to be an efficient method for that: this method allows to determine a seismic velocity distribution from traveltimes data associated with the seismic waves reflecting on geological surfaces. This inverse problem is formulated as a least-square minimization problem which consists in the minimization of the mismatch between the observed traveltimes and the traveltimes computed by the forward problem (solved by a ray tracing method). The first section of this paper presents an overview of the reflection tomography method we have developed ([10], [11], [13], [9]).

Methods for the a posteriori analysis of the solution are then proposed and applied on a 2D real data set. Indeed, classically, the analysis of the solution consists only in checking the misfits between observed traveltimes and calculated traveltimes by computing characteristic values of the misfit distribution and by studying the spatial distribution of the misfits. This analysis is not sufficient: even if these quality control criteria are matched, the determined model is only one of many possible models that match the data. An uncertainty analysis should be performed to quantify the range of admissible models we can obtain from these data and the a priori information ([6]).

The different methods described here allow to access the uncertainties on the solution model thanks to the analysis of the a posteriori covariance matrix ([7], [14]) obtained in the linearized framework. The computation of this matrix is generally expensive for 3D problems and the physical interpretation of its terms may be cumbersome. The simulation of admissible models from the a posteriori probability density function allows a more complete analysis than the sole analysis of the diagonal terms of the a posteriori covariance matrix and furnishes directly physical models. This method requires a Cholesky decomposition of the Gauss-Newton matrix which may be unfeasible for 3D realistic models. To overcome this difficulty, we propose a formalism based on linear combinations of model parameters (macro-parameters) that allows to compute uncertainties on relevant geological quantities (the average thickness of a layer for example) for a reduced computational time (the a posteriori covariance matrix is reduced to the macro-parameter space). The application of these methods on a real data set shows their effectiveness and their limitations are discussed, particularly the limitations due to the linearization: a non linear approach is proposed in order to delimit the space of admissible solutions.

## 2 THE REFLECTION TOMOGRAPHY PROBLEM

Let us first present the reflection tomography method which was developed in KIM consortium ([9]). The chosen model representation is a *blocky* velocity model where the velocity distribution is described by slowly varying layer velocities (also called velocity blocks) delimited by interfaces (see Figure 1 for an example). The model is thus composed of two kinds of parameters: parameters describing the velocity variations within the layers

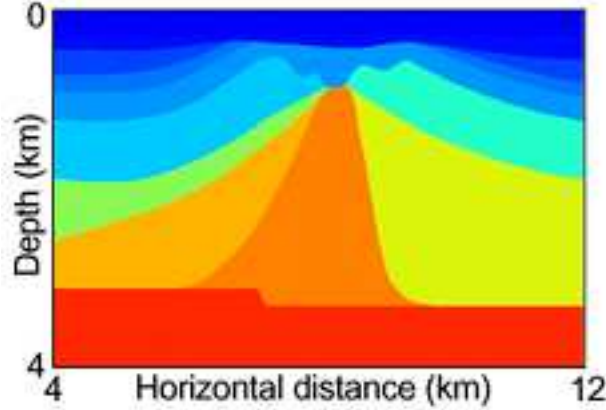


Figure 1: An exemple of a *blocky* subsurface model.

and parameters describing the geometry of the interfaces delimiting the velocity blocks<sup>1</sup>. Moreover, anisotropy of the velocity may be modelled by two parameters  $\eta$  and  $\delta$  (see [13] for more details). This *blocky* representation allows the representation of complex models (e.g. presenting rapid lateral velocity variations and complex geological structures) with a reasonable number of unknowns. A strong a priori information is introduced, the number of layer being fixed: this reduces the underdetermination of the inverse problem.

The forward problem of reflection tomography consists in computing traveltimes of reflected seismic waves, given a model, an acquisition survey (locations of the sources and the receivers) and signatures (reflectors where the waves reflect). It is solved by a ray tracing method which is a high frequency approximation of the wave equation ([11]). We denote by  $T(m)$  the forward modeling operator, that is the operator that gives, for a specified reflector, the traveltimes associated with all source-receiver pairs.

Reflection travelttime tomography is the corresponding inverse problem: its purpose is to adjust  $m$  such that  $T(m)$  best matches a vector of traveltimes  $T^{obs}$  picked on seismic data. A natural formulation of this problem is the least squares formulation

$$\| T(m) - T^{obs} \|_{C_D^{-1}}^2 + \| m - m^{prior} \|_{C_M^{-1}}^2, \quad (1)$$

where

- $C_D$  is the a priori covariance operator in the data space that allows to describe errors on the data,
- $m^{prior}$  is an a priori model (coming, for instance, from geological knowledge and/or additionnal information resulting from well measurements),

---

<sup>1</sup>In our approach ([10]), the subsurface model  $m$  is composed of 2D or 3D B-spline functions describing velocity variations in a layer ( $v(x, y) + k.z$  or  $v(x, y, z)$ ) and 2D B-spline functions describing the interfaces ( $Z(x, y)$ ,  $Y(z, x)$  or  $X(y, z)$ ).

- $C_M$  is the a priori covariance matrix in the model space that allows to describe errors on the a priori model.

In practice, building an a priori model is difficult and the a priori term, which is necessary to well pose the inverse problem, is often replaced by regularization terms made up of second derivatives of the model ([5]) which leads to  $C_M^{-1} = \mathcal{Q}_{reg}$  and  $m^{prior} = 0$

$$\| T(m) - T^{obs} \|_{C_D^{-1}}^2 + \epsilon^2 \| D^2 m \|^2 \quad (2)$$

where a continuation technique ([3]) is applied for tuning the regularization weight  $\epsilon$ : the weight is decreased until the model matches the data with the expected accuracy. The obtained model is then the smoothest model which fits the data. This methodology allows to stabilize the inversion.

This large size non linear least-square problem (the objective function is not quadratic since the forward modeling operator  $T(m)$  is non linear) is solved classically by a Gauss-Newton method based on successive linearizations of the forward operator which needs the computation of the Jacobian matrix of  $T$  ( $J(m) = \frac{\partial T}{\partial m}(m)$ )<sup>2</sup>. The resulting approximation of the Hessian is noted  $H(m) = J(m)^t C_D^{-1} J(m)$ .

The resulting quadratic approximation of the objective function (2)

$$\tilde{C}_n(\delta m) = \| J_n \delta m - \delta T_n^{obs} \|_{C_d^{-1}}^2 + \epsilon^2 \| D^2(m_n + \delta m) \|^2 \quad (3)$$

is minimized at each Gauss-Newton iteration  $n$  by a preconditionned conjugate gradient ( $m_n$  is the current model,  $\delta m$  is the model perturbation,  $J_n = \frac{\partial T}{\partial m}(m_n)$  is the Jacobian matrix evaluated at  $m_n$ , and  $\delta T_n^{obs} = T^{obs} - T^{cal}(m_n)$ ) ([4]).

### 3 PRESENTATION OF THE APPLICATION

Let us consider a 2D PP/PS<sup>3</sup> real data set studied by [2]. 45338 traveltimes data were interpreted and an uncertainty of 5ms (resp. 8ms) are associated with PP data (resp. PS data). A layer-stripping approach (separate inversion of each velocity layer from the shallower layer to the deeper one) furnished the velocity model of Figure 2. The model is described by four interfaces, corresponding to the interpreted events ( $h_1$ ,  $h_3$ ,  $h_4$  et  $h_5$ ) which define only three layers with lateral velocity variations for the two first upper layers ( $v(x)$ , there is no vertical variations) and the last layer stretching from  $h_3$  to  $h_5$  with a 2D velocity  $vp_5(x, z)$  and  $vs_5(x, z)$  (Figure 2). This model is composed of 4588 parameters, 592 for the interfaces and 3936 for the velocities. Anisotropy in the deepest layer is parameterized by  $\eta$  and  $\delta$  ([2]) which are assumed constant per layer ( $\eta$  can

<sup>2</sup>The computation of the derivatives of  $T$  with respect to the model parameters is cheap, thanks to the Fermat principle ([1]).

<sup>3</sup>PS-wave results from the conversion at the reflector of a down-going P-wave (compressional wave) into an up-going S-wave (shear wave). In opposition to the PS-wave, the pure P mode is often called the PP-wave.

be seen as a measure of the velocity an-ellipticity, whereas  $\delta$  controls the near vertical velocity propagation of the P-waves). For the two first layers, the inversion results are very satisfactory, with a travelttime misfit RMS (root mean square) of  $3.5ms$  for the PP-data and of  $7ms$  for the PS-data. For the last layer, the travelttime misfit RMS is of  $3.7ms$  and of  $5.6ms$  for, respectively,  $h4$  and  $h5$  PP-data and of  $8.5ms$  for  $h5$  PS-data, results which are consistent with the data uncertainties (Figure 3).

As already shown by [13], it turns out that the anisotropy parameter  $\delta$  is strongly undetermined from seismic data. The value of  $\delta$  parameter was obtained by a trial and error approach in order to match approximatlty the depth of  $h5$  horizon given at well location. We propose then to carry on an a posteriori uncertainty analysis in order to quantify the uncertainties on this solution model: we focus on the anisotropic layer delimited by  $h3$  and  $h5$  (velocities  $vp5$  and  $vs5$ ).

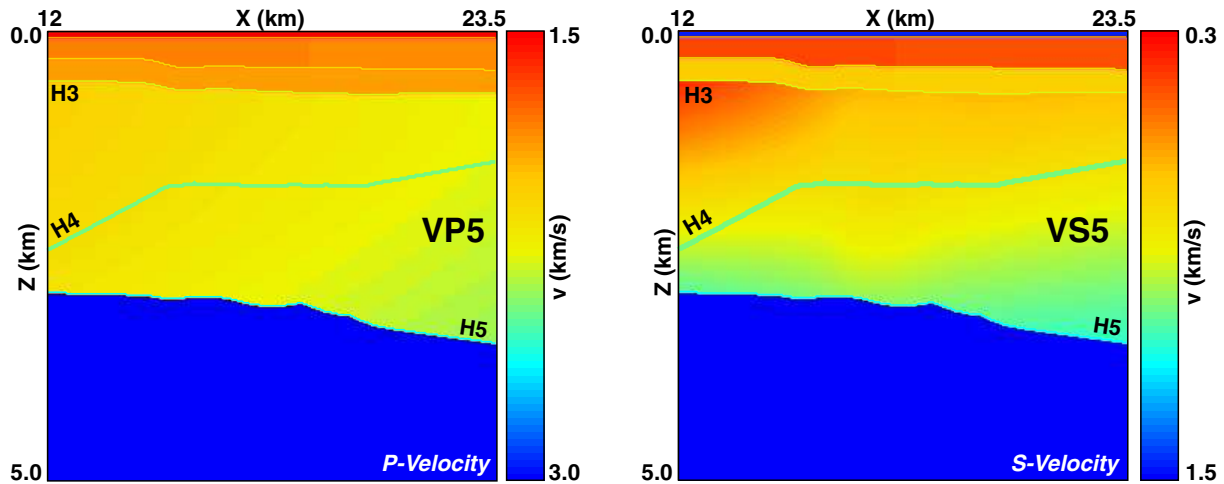


Figure 2: Solution velocity model obtained by tomography. Left: P velocity. Right: S velocity. The RMS value of the travelttime misfits is  $6.2ms$ . The anisotropy parameters values are:  $\eta = 6.29\%$  and  $\delta = -4.43\%$ .

#### 4 QUANTIFYING UNCERTAINTIES ON THE SOLUTION MODEL: A LINEARIZED APPROACH

A classical approach to quantify uncertainties consists in the analysis of the Hessian matrix (or its inverse: the a posteriori covariance matrix) associated with the linearized problem (3) around the solution  $m_\infty$ . This approach is valid in the vicinity of the solution model, the size of the vicinity depending on the non-linearity of the forward map.

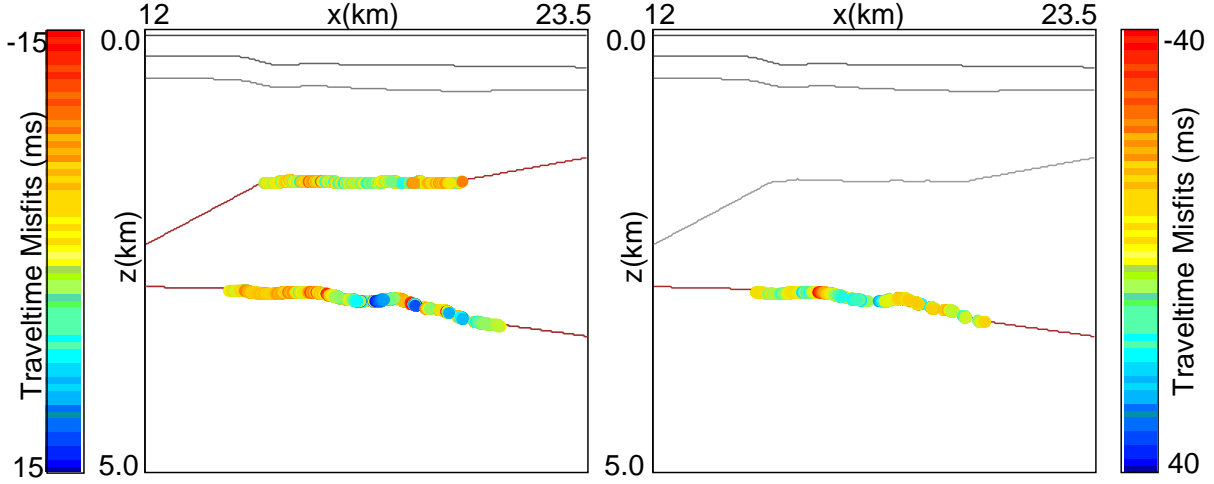


Figure 3: Interfaces of the solution velocity model obtained by tomography and their associated traveltime misfits: impact points of rays reflected on  $h_4$  and  $h_5$  (Left: PP rays. Right: PS rays), colors represent travelttime misfits. Notice that the illuminated zone extends from  $14\text{ km}$  to  $20.5\text{ km}$ .

The bi-linear form associated with the Hessian matrix measures the influence of a model perturbation  $\delta m$  on the quadratic cost function defined around the solution  $m_\infty$ :

$$\begin{aligned} \tilde{C}(\delta m) - \underbrace{\tilde{C}(0)}_{=C(m_\infty)} &= \frac{1}{2}(J(m_\infty)\delta m)^T C_D^{-1}(J(m_\infty)\delta m) + \frac{1}{2}\delta m^T C_M^{-1}\delta m \\ &\quad - \delta m^T \underbrace{(J(m_\infty)^T C_D^{-1}\delta T^{obs}(m_\infty) - C_M^{-1}m_\infty)}_{=g(m_\infty)=0, \text{ gradient of } C(m) \text{ vanishes at the solution } m_\infty} \\ &= \frac{1}{2}\delta m^T (J(m_\infty)^T C_D^{-1}J(m_\infty) + C_M^{-1})\delta m \end{aligned} \quad (4)$$

$$= \frac{1}{2}\delta m^T H(m_\infty)\delta m. \quad (5)$$

The a posteriori covariance matrix is defined by

$$C'_M = (J(m_\infty)^T C_D^{-1}J(m_\infty) + C_M^{-1})^{-1}. \quad (6)$$

The space of admissible models can be characterized by the contour lines

$$(m - m_\infty)^T C_M'^{-1}(m - m_\infty) = constant, \quad (7)$$

which are ellipsoïds of center  $m_\infty$  and correspond also to contour lines of the a posteriori Gaussian probability density function

$$\exp\left(-\frac{1}{2}\delta m^T C_M'^{-1}\delta m\right). \quad (8)$$

The diagonal terms of  $C'_M$  are the uncertainties on the parameters describing the model and the off-diagonal terms are the correlations between these uncertainties. For instance, the probability that the true model parameter  $p_i$  verifies  $-2C'_{M,i,i} \leq p_i - p_\infty \leq 2C'_{M,i,i}$ , independently of the values of the other model parameters, is about 95%. To take into account the correlations between the parameters, we should study the 95% confidence ellipsoid. The axes of the ellipsoids (7) are defined by the eigenvectors of  $C'_M$ , the square root of the eigenvalues giving the uncertainties on the associated eigenvector.

We propose in the next sections two methods to quantify geological uncertainties on the solution model which avoid the expensive computation and the cumbersome analysis of the generally huge a posteriori covariance matrix  $C'_M$ .

#### 4.1 Simulations of admissible models

The first proposed method to quantify uncertainties is the simulation of admissible models from the a posteriori probability density function (8) (pdf). The simulations furnish directly interpretable results, i.e. physical models. The method (see for instance [12]) consists in random simulations of model perturbations following the pdf (8).

First, we apply the variable transformation:

$$\delta m' = U\delta m, \quad (9)$$

where  $U$  is the lower triangular matrix obtained by a Cholesky decomposition of the inverse of the a posteriori covariance matrix  $C'^{-1}_M = H = U^T U$  (symmetric semi positive definite matrix). The method consists then in simulations of the uncorrelated Gaussian pdf with unit variance

$$\exp\left(-\frac{1}{2}\delta m'^T \delta m'\right). \quad (10)$$

Simulations  $\delta m'$  are transformed into correlated Gaussian simulations of vector  $\delta m$  by the inverse transformation of (9).

Figures 4, 5, 6, 7 and 8 show 100 simulated models obtained by this method from the solution model of Figure 2: interfaces  $h4$  and  $h5$ , variations of velocities  $vp5$  and  $vs5$  along  $x$  and  $z$  directions and histograms of the anisotropy parameters  $\eta$  and  $\delta$ . From these simulations, we observe that the highest uncertainties on the lateral velocity variations are located at the boundaries of the model, areas that are not well illuminated by the rays. Indeed, for a slice at constant  $z = 2.7km$ , we observe uncertainties of  $\approx 690m/s$  for  $vp5$  and of  $\approx 260m/s$  for  $vs5$  at the boundaries of the model and uncertainties of  $\approx 450m/s$  for  $vp5$  and of  $\approx 140m/s$  for  $vs5$  in the illuminated parts of the model. Concerning the interface depths, we observe uncertainties of  $\approx 180m$  for reflector  $h4$  and of  $\approx 220m$  for reflector  $h5$  at the boundaries and of  $\approx 90m$  for reflector  $h4$  and of  $\approx 100m$  for reflector

$h5$  elsewhere. For the anisotropy parameters  $\eta$  and  $\delta$ , we notice uncertainties around 0.3% on  $\eta$  and 2% on  $\delta$ . This method is quite attractive for the straightforward interpretation of the results despite its cost (cost of the Choleski decomposition): it furnishes physical models leading to small perturbations of the quadratic cost functions (3) (see Table 4.3).

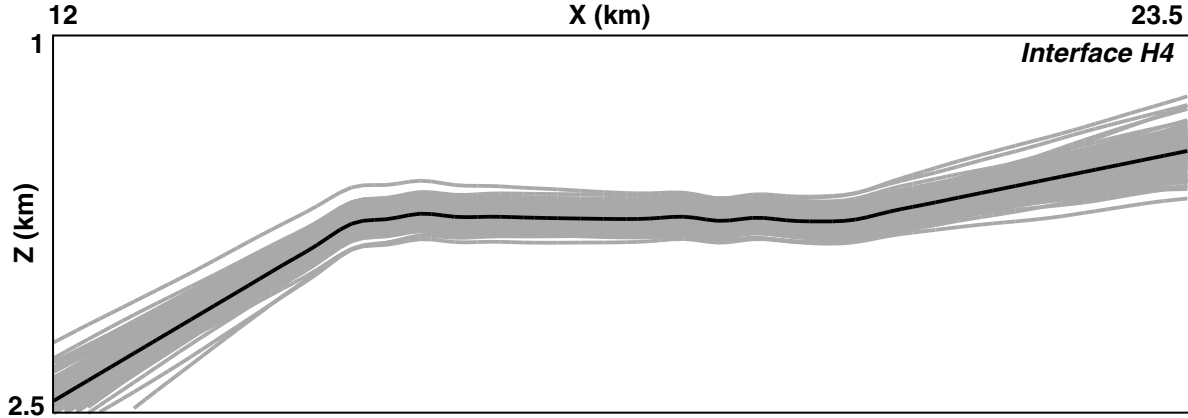


Figure 4: Reflector  $h4$  extracted from the 100 simulated velocity models. The bold line represents the solution interface.

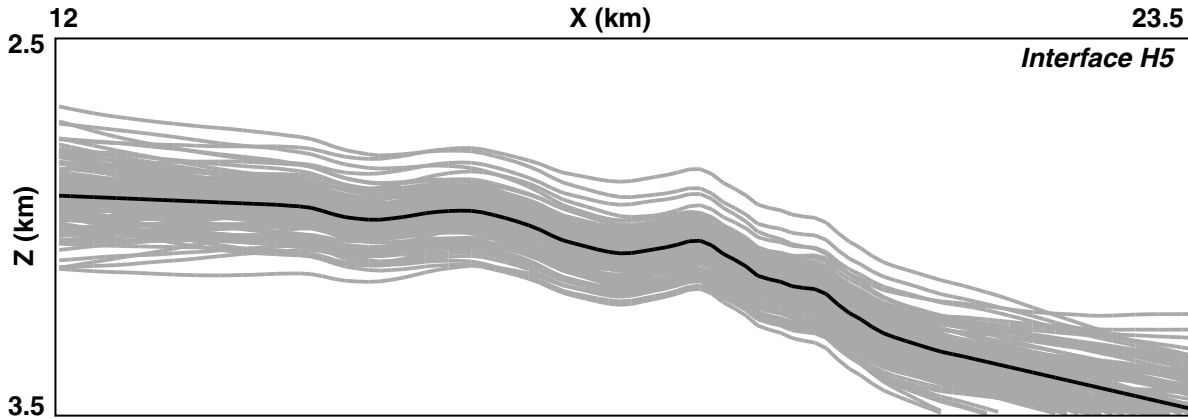


Figure 5: Reflector  $h5$  extracted from the 100 simulated velocity models. The bold line represents the solution interface.

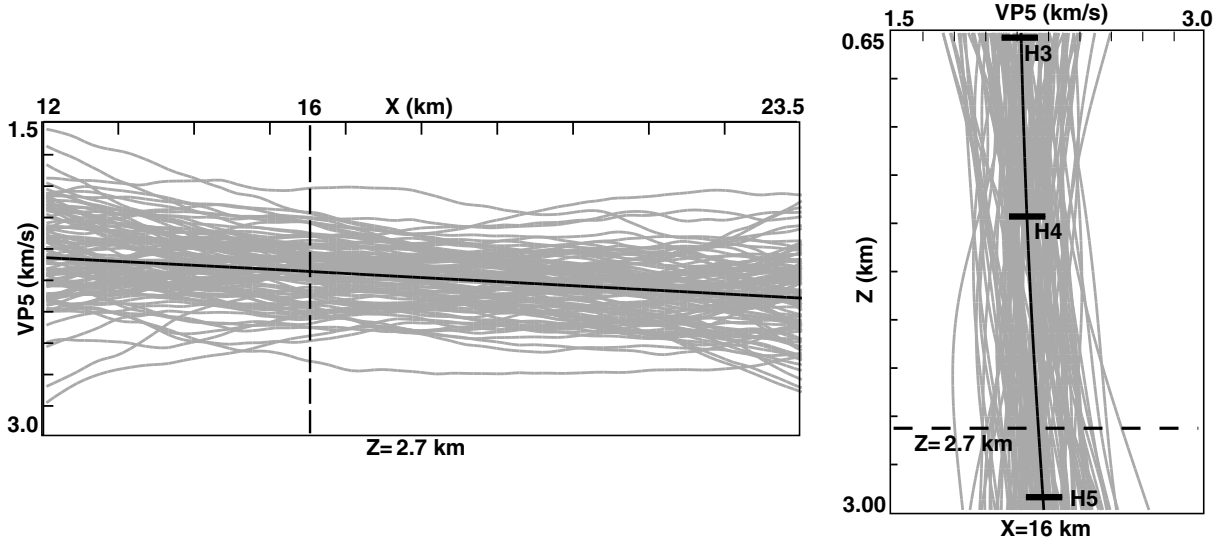


Figure 6: P-velocity variations along  $x$  axis at  $z = 2.7\text{km}$  (left) and along  $z$  axis at  $x = 16\text{km}$  (right) extracted from the 100 simulated velocity models.

#### 4.2 Uncertainties on geological macro-parameters

We propose here a method that allows to deal with large size models at a reasonable cost and furnishes uncertainties on chosen physical quantities. The proposed approach consists in building macro-parameters (MP) with a geophysical interest. These macro-parameters are linear combinations of the inverted parameters such as the mean of the velocity variations in a zone, the slope of an interface, the average thickness of a layer, etc. [8] has introduced the notion of macro-parameter (his main motivation being to avoid numerical problems in the inversion of the complete Hessian). We propose here a generalization of his work (general definition of macro-parameters) which allows the computation of uncertainties for huge 3D problems.

We define a macro-parameter as:

$$P = Bp, \quad (11)$$

where  $p$  is the  $np$  model parameters vector,  $P$  is the  $n_{MP}$  macro-parameters vector and  $B$  is the condensation matrix. We compute the a posteriori covariance matrix  $\tilde{C}'_M$  in the macro-parameter space:

$$\tilde{C}'_M = BC'_M B^T. \quad (12)$$

Note that  $\tilde{C}'_M$  (a  $n_{MP} \times n_{MP}$  matrix) is small compared to  $C'_M$  (a  $n_p \times n_p$  matrix) since  $n_{MP} \ll n_p$ . To obtain this matrix, we do not need to compute the whole inverse of the Hessian,  $C'_M = H^{-1}$ , in the parameter space. Indeed, to obtain  $\tilde{C}'_M = \tilde{H}^{-1} = BH^{-1}B^T$  in

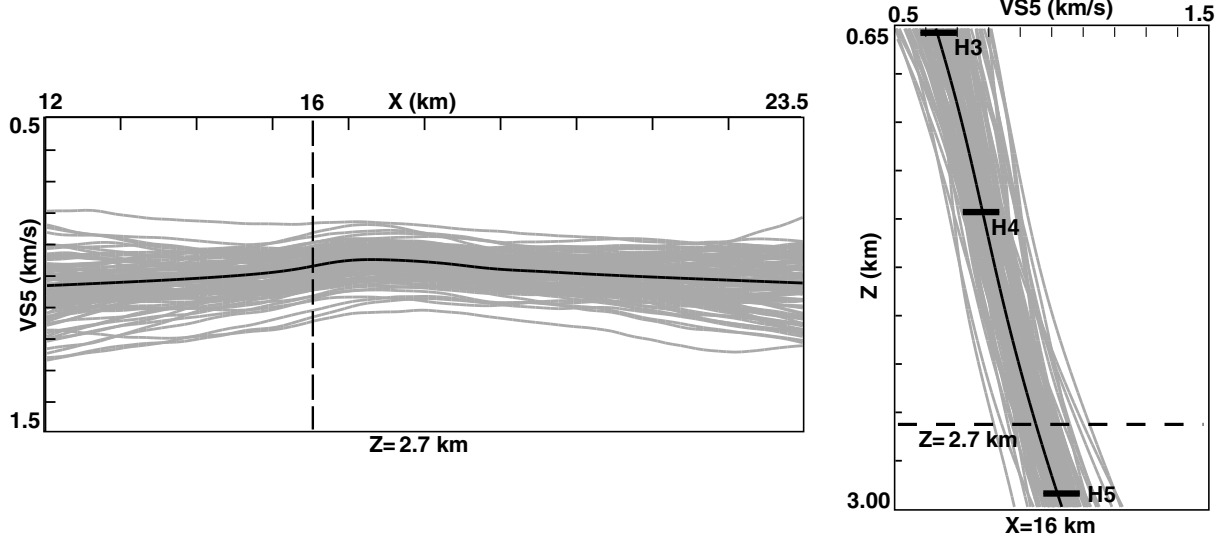


Figure 7: S-velocity variations along  $x$  axis at  $z = 2.7\text{km}$  (left) and along  $z$  axis at  $x = 16\text{km}$  (right) extracted from the 100 simulated velocity models.

the MP space, we just need  $H^{-1}B_j^T$ , where  $B_j^T$  are the different columns of  $B^T$ . We thus solve  $n_{MP}$  linear systems,  $\tilde{H}_j^{-1} = BH^{-1}B_j^T$ , that are similar to the linearized problem we solve at each Gauss-Newton iteration. Thus the computational cost for one MP is comparable to one iteration of the inversion process.

We applied this method on the model of Figure 2. We choose simple MP: the mean of the velocity variations and the mean of the interface depth in the illuminated part of the layer (region covered by rays)<sup>4</sup>. The results are listed in the Table 1. The uncertainty on anisotropy parameter  $\delta$  is high:  $\pm 3.2\%$  (if we consider twice standard deviation) and we observe high correlations between  $\eta$  and  $\delta$  (0.93) and also correlations between anisotropy parameters and  $H5$  depth ( $-0.33$  and  $-0.36$ ). We notice also the bad determination of the velocities:  $\pm 22\%$  (relative value). All these results are consistent with the simulations results (section 4.1).

This method with its general formalism allows to compute uncertainties on relevant geological quantities with a reasonable computation cost and to highlight easily strong coupling between the chosen MP.

### 4.3 Discussions on the two methods

As already mentioned, the two methods described in sections 4.1 and 4.2 rely on the quadratic approximation (3) of the non linear cost function. In the table 4.3 we have listed the RMS of traveltime misfits for 20 simulated models. Note that the RMS traveltime

<sup>4</sup>From figure 3, we define the illuminated region by  $x \in [14, 20.5\text{km}]$ .

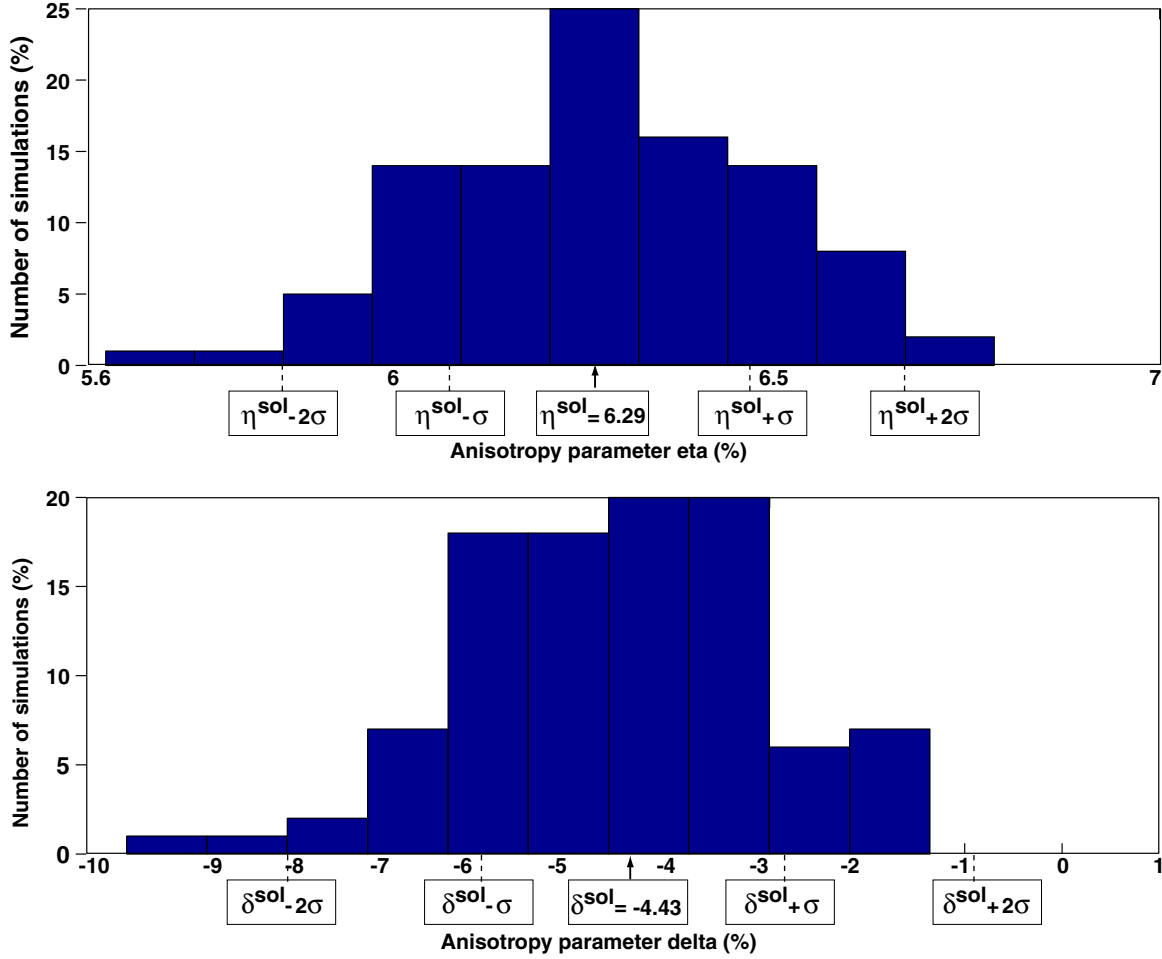


Figure 8: Histograms of the 100 simulated velocity models. Top: anisotropy parameter  $\eta$ . Bottom: anisotropy parameter  $\delta$ .  $\sigma$  corresponds to the standard deviation on the anisotropy parameter  $\eta$  ( resp.  $\delta$ ) given by the macro-parameter method.(see section 4.2).

misfit for the solution model is  $6.2ms$ . Thus, there is only one model which is not acceptable ( $11.6ms$  for the model 15), the others are admissible models with a RMS travelttime misfit bounded by  $7ms$ . The simulation method has then furnished model perturbations that correspond to small perturbations of the quadratic cost function but also to small perturbations of the non linear cost function (RMS of travelttime misfits remain small). It shows for this example, the good concordance between the quadratic cost function and the non linear one around the solution model.

Figure 9 illustrates isovalues of the probability density function (8) in the MP space, i.e. ellipsoids defined by  $\delta m_{MP}^T \tilde{C}_M'^{-1} \delta m_{MP}$ : we visualize the 2D-marginal probability density functions for several relevant MP couples, the 68% confidence ellipsoid and the 95% confidence ellipsoid for  $\eta$  and  $\delta$ ,  $vp5$  and  $vs5$ ,  $\delta$  and  $h5$ . This representation allows to

	<b><i>Vp5</i></b>	<b><i>Vs5</i></b>	<b><i>η</i></b>	<b><i>δ</i></b>	<b><i>H4</i></b>	<b><i>H5</i></b>
<b><i>Vp5</i></b>	<b><i>475.1 m/s</i></b> <i>(22%)</i>	0.002	-0.03	-0.02	0.005	0.01
<b><i>Vs5</i></b>	0.002	<b><i>168.9 m/s</i></b> <i>(22%)</i>	-0.04	-0.03	0.005	0.01
<b><i>η</i></b>	-0.03	-0.04	<b><i>0.22%</i></b> <i>(4%)</i>	<b><i>0.93</i></b>	-0.16	<b><i>-0.33</i></b>
<b><i>δ</i></b>	-0.02	-0.03	<b><i>0.93</i></b>	<b><i>1.6%</i></b> <i>(37%)</i>	-0.17	<b><i>-0.36</i></b>
<b><i>H4</i></b>	0.005	0.005	-0.16	-0.17	<b><i>77.1 m</i></b> <i>(5%)</i>	0.06
<b><i>H5</i></b>	0.01	0.01	<b><i>-0.33</i></b>	<b><i>-0.36</i></b>	0.06	<b><i>80.3 m</i></b> <i>(3%)</i>

Table 1: Standard deviations in bold (square roots of the diagonal terms of the a posteriori covariance matrix) associated with the MP "mean in the illuminated part of the model" and the normalized correlations between the uncertainties on the different defined MP. This uncertainty analysis is performed for the solution model of Figure 2. The normalized values  $\frac{\sigma}{|value^{sol}|} \times 100$  of the standard deviations ( $\sigma$ ) are also indicated in italic.

underline the correlations between the anisotropy parameters  $\eta$  and  $\delta$  which are quite strong in this example: the 68% and the 95% confidence ellipsoids are elongated (left part of the figure 9). On the opposite, the P and S velocities are uncorrelated: we obtain almost a circle (middle part of the figure 9). We can also observe correlations between the anisotropy parameter  $\delta$  and the mean of the last reflector depth  $h5$  (right part of the figure 9). On this Figure, we have also superimposed the anisotropy parameters  $\eta$  and  $\delta$  and the MP  $vp5$  and  $vs5$ ,  $\delta$  and MP  $h5$  built from the 100 simulated models. This figure allows to point out the equivalence of the simulation method and the macro-parameter approach.

Note that the macro-parameter approach furnishes interesting information on the correlations of macro-parameter uncertainties and has a lower computation cost than simulations of the model parameters with the complete a posteriori covariance matrix. We could also perform gaussian simulations of the macro-parameters using the reduced a posteriori covariance matrix.

## 5 NON-LINEAR A POSTERIORI ANALYSIS

We have shown in the previous sections that a linearized uncertainty analysis allows to delimit the range of possible solution models that fit, with the expected accuracy, the data

<b>Models</b>	<b>RMS(ms)</b>	<b>vp5(km/s)</b>	<b>vs5(km/s)</b>	<b>h4(km)</b>	<b>h5(km)</b>	<b><math>\eta(\%)</math></b>	<b><math>\delta(\%)</math></b>
<b>1</b>	6.7	3.736	1.154	1.783	3.131	6.5	-2.6
<b>2</b>	6.6	3.121	1.222	1.925	3.222	6.2	-4.9
<b>3</b>	6.4	2.746	1.102	1.790	3.060	6.0	-5.9
<b>4</b>	6.9	2.701	1.315	1.857	3.259	6.2	-3.7
<b>5</b>	6.2	3.300	1.416	1.817	3.142	5.7	-8.3
<b>6</b>	6.5	2.542	1.245	1.926	3.181	6.1	-4.6
<b>7</b>	6.6	2.536	1.137	1.925	3.143	6.1	-5.5
<b>8</b>	6.2	1.919	1.087	1.844	3.102	6.3	-4.8
<b>9</b>	6.2	3.182	1.078	1.875	3.267	6.5	-3.5
<b>10</b>	6.4	2.960	1.388	1.736	3.198	6.0	-6.2
<b>11</b>	6.2	3.247	1.452	1.815	3.173	6.0	-6.4
<b>12</b>	6.2	2.592	1.073	1.664	3.147	6.6	-1.4
<b>13</b>	6.5	2.510	1.239	1.817	3.239	6.2	-4.9
<b>14</b>	6.6	3.595	1.130	1.717	3.208	6.5	-1.9
<b>15</b>	11.6	2.344	1.172	1.770	3.144	6.0	-6.1
<b>16</b>	6.5	2.154	1.323	1.853	3.2322	6.3	-4.5
<b>17</b>	6.3	2.855	1.307	1.797	3.296	6.3	-3.4
<b>18</b>	6.2	2.125	1.049	1.921	3.118	5.9	-6.8
<b>19</b>	6.6	1.431	1.048	1.772	3.144	6.4	-3.7
<b>20</b>	6.3	2.371	1.225	1.864	3.166	6.0	-6.6

Table 2: RMS values of the traveltimes misfits, mean value of the velocities  $vp5$  and  $vs5$ , of the interfaces  $h4$  and  $h5$  in illuminated region (MP defined in section 4.2 and anisotropy parameters  $\eta$  and  $\delta$  for 20 simulated models (chosen among the 100 simulations presented in section 4.1).

and the a priori information. Nevertheless, we should keep in mind that this approach is only valid in the vicinity of the solution model (linearized framework) and complex cases may require a non linear approach.

Model 15 of table 4.3 indicates that some of the simulated models may produce unacceptable traveltimes misfits ( $RMS \approx 11ms$  and  $MAX = 25ms$  for PP data and  $= 41ms$  for PS data). It shows the limitation of the quadratic approximation of the non linear cost function and thus the limitation of the linearized methods of uncertainty quantification. Moreover, [4] has shown that a tomographic inversion with constraints on the location of the interfaces at well locations furnished a very different model (model 2 of Figure 10) than the solution model of Figure 2. The two models verify the traveltime data with the expected accuracy. This second model does not belong to the range of possible models detected by the two methods we proposed: indeed,  $\delta$  is equal to 15.94% whereas the expected range of values was between -8% and -1% (see for instance Figure 8). It shows

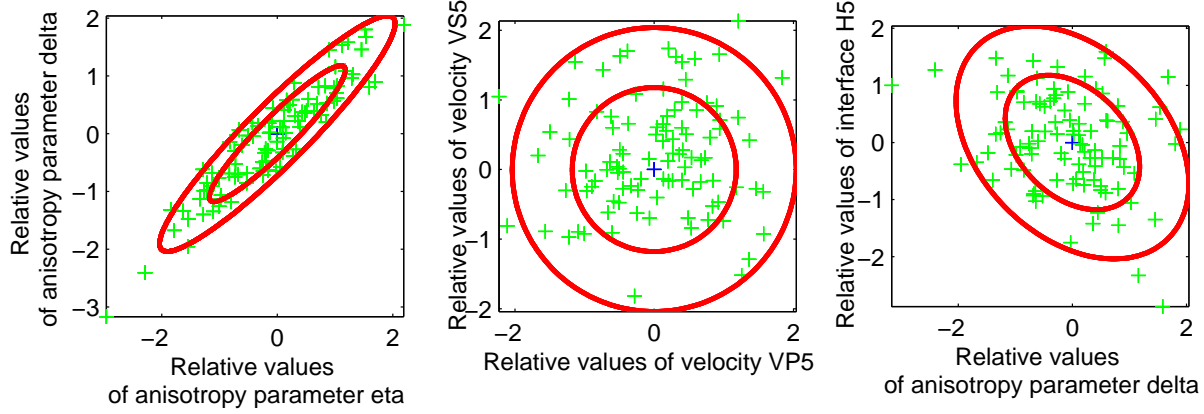


Figure 9: 68% and 95% isovalues of the marginal probability density function for the anisotropy parameters  $\eta$  and  $\delta$  (left), P-velocity and S-velocity (middle),  $\delta$  and the interface depth of reflector h5 (right). The represented values are the relative ones (for instance:  $\frac{\eta - \eta_{sol}}{|\sigma_\eta|}$ , where  $\sigma_\eta$  is the standard deviation for the anisotropy parameter  $\eta$ ). The crosses represent the MP values of the 100 simulated models.

again the limitations of the linearized approach.

To perform a non linear analysis we have chosen an experimental approach which consists in performing several inversions allowing to test different geological scenarii to try to delimit the space of admissible solutions. For instance, we could test different hypothesis on the values of the anisotropy parameters for which a strong uncertainty has been detected by the linearized approach. If we introduce a constraint on the anisotropy parameter  $\delta$ , such as  $\delta > 0$ , we find the model 3 displayed in Figure 11: this result expands the range of admissible models (variability of  $\delta$  detected by MP approach was  $-4.43 \pm 3.2\%$ ). In the same way, we can test the variability of the anisotropy parameter  $\eta$ . We notice (see table 5) that the value of the anisotropy parameter  $\eta$  of the model 2 (Figure 10) is 8.27%, but all the simulated values of this parameter are around 6% and the variability of  $\eta$  furnished by the MP is 0.44%. Nevertheless, tomographic inversion under the constraint  $\eta \leq 4\%$  or  $\eta \geq 8\%$  does not furnish a model that satisfies both these constraints and the data with the expected accuracy. We have shown that, by constrained tomography, we can test different geological hypothesis and delimit the space of admissible models and go further than the linearized approach which explores only the vicinity of the solution model which may be one local minimum around others.

	<i>Model 1</i>	<i>Model 2</i>	<i>Model 3</i>
<i>mean of the P-velocity</i>	2.849 km/s	3.623 km/s	2.895 km/s
<i>mean of the S-velocity</i>	1.229 km/s	1.621 km/s	1.213 km/s
$\eta$	6.29%	8.27%	6.2%
$\delta$	-4.4%	15.94%	2%
<i>mean of the depth of the reflector H4</i>	1.838 km	1.755 km	1.659 km
<i>mean of the depth of the reflector H5</i>	3.167 km	3.021 km	2.882 km

Table 3: 3 different solution models. Model 1 is the model of Figure 2, Model 2 is the model of Figure 10 and Model 3 is the model of Figure 11.

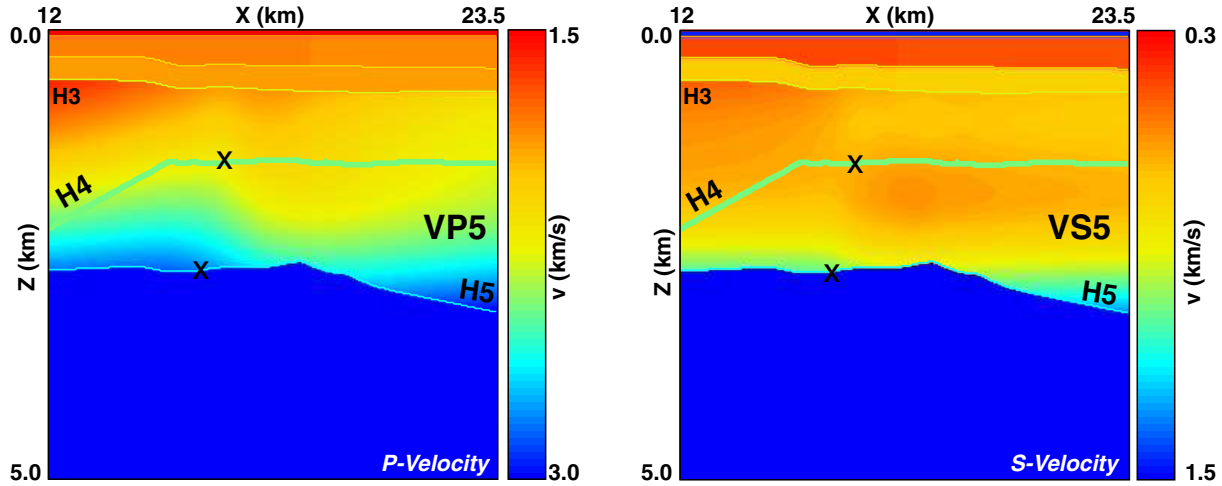


Figure 10: Solution model 2 obtained by tomography with additional constraints on the interface depth at well locations. The RMS value of the traveltime misfits is 6.0ms. The anisotropy parameters values are:  $\eta = 8.27\%$  and  $\delta = 15.94\%$ . The crosses represent the wells.

## 6 CONCLUSIONS

Reflection tomography furnishes the velocity model that best fits the travelttime data; however, this solution is only one among many admissible models. An a posteriori uncertainty analysis is crucial to delimit the range of possible solution models that would fit the data and the a priori information with the expected accuracy. In this paper, we describe two methods to perform a linearized a posteriori analysis, approach valid only in the vicinity of the solution model. The simulation method based on the analysis of the a posteriori covariance matrix (huge matrix for 3D models) is quite attractive for the straightforward interpretation of the results despite its cost. We propose a general formalism to reduce the a posteriori analysis to geological quantities of the model: we evaluate uncertainties on macro-parameters (linear combinations of model parameters) that have a geological interest. This method allows the manipulation of reduced matrices

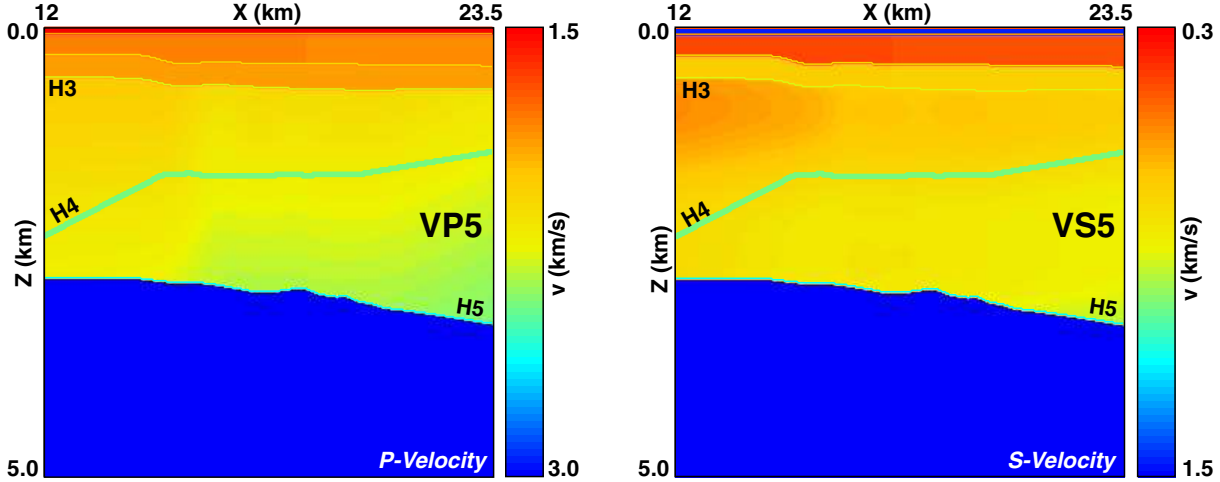


Figure 11: Solution model 3 obtained by tomography with a constrain on  $\delta$  parameter to remain positive. The RMS value of the traveltimes misfits is  $6.371ms$ . The anisotropy parameters values are:  $\eta = 6.2\%$  and  $\delta = 2\%$ .

and thus becomes feasible in 3D. Nevertheless, we have confirmed on this real data set that this approach is only valid in the vicinity of the solution model (linearized framework) and that some cases require a non linear approach to search for local minima of the cost function. An experimental approach has consisted in solving the inverse problem under constraints (for instance constraints on anisotropy parameters) to test the validity of some geological hypothesis.

## 7 ACKNOWLEDGMENTS

The authors would like to thank bp to have provided the data set, Karine Broto and Frédéric Delbos for many fruitful discussions.

## REFERENCES

- [1] T. N. Bishop, K. P. Bube, R. T. Cutler, R. T. Langan, P. L. Love, J. R. Resnick, R. T. Shuey, D. A. Spindler and H. W. Wyld. Tomographic determination of velocity and depth in laterally varying media, *Geophysics*, **50**, no 6, 903–923, 1985.
- [2] K. Broto, A. Ehinger and J. Kommedal. Anisotropic traveltime tomography for depth consistent imaging of PP and PS data, *The leading Edge*, 114–119, 2003.
- [3] K. P. Bube and R. T. Langan. A continuation approach to regularization for travelttime tomography. In *Expanded Abstracts*, 980–983, 64<sup>th</sup> Ann. Internat. Mtg., Soc. Expl. Geophys., 1994.
- [4] D. Sinoquet, F. Delbos and J.C. Gilbert. A dedicated constrained optimization method for 3D reflection tomography. In *Expanded Abstracts*. EAGE 66<sup>th</sup> conference and exhibition, 2004.
- [5] F. Delprat-Jannaud and P. Lailly. Ill-posed and well-posed formulations of the reflection travelttime tomography problem. *Journal of Geophysical Research*, **98**, 6589–6605, 1993.
- [6] C. Duffet and D. Sinoquet. Quantifying geological uncertainties in velocity model building. In *Expanded Abstracts*, 926–929, 72<sup>nd</sup> Ann. Internat. Mtg., Soc. Expl. Geophys., 2002.
- [7] W. P. Gouveia and J.A. Scales. Resolution of seismic waveform inversion: bayes versus occam. *Inverse problems*, 323–349, 1997.
- [8] D. Grenié. *Tomographie de temps de trajet adaptée au problème de l'imagerie 3D en exploration pétrolière: théorie, mise en oeuvre logicielle et applications*. Ph.D. thesis, Université Paris VII, 2001.
- [9] <http://consortium.ifp.fr/KIM/>, 2001, *Web pages of former KIM consortium*.
- [10] F. Jurado, D. Sinoquet and A. Ehinger. 3D reflection tomography designed for complex structures. In *Expanded Abstracts*, 711–714, 66<sup>th</sup> Ann. Internat. Mtg., Soc. Expl. Geophys., 1996.
- [11] F. Jurado, P. Lailly and A. Ehinger. Fast 3D two-point raytracing for travelttime tomography. Proceedings of SPIE, *Mathematical Methods in geophysical Imaging*. Vol. V, **3453**, 70–81, 1998.
- [12] R. Parker. *Geophysical inverse theory*. Springer, Berlin, 1994.

- [13] A. Stopin. Reflection tomography of compressional and shear modes for determination of anisotropic velocity models: Phd Thesis of Université Louis Pasteur, Strasbourg I, 2001.
- [14] A. Tarantola. *Inverse problem theory*. Elsevier, 1987.